International Journal of Control and Automation
Vol. 8, No. 1 (2015), pp. 1-8
http://dx.doi.org/10.14257/ijca.2015.8.1.01

Efficiency Optimization Control for Three-Phase Induction Motors with Hall Sensor

Xifeng Wang[1.2], Dawei Meng[1] and Yongming Xu[1]

[1]*College of Electrical and Electronic Engineering, Harbin University of Science and Technology.Harbin, 150080, P.R. China.*
[2]*College of Electrical and Information Engineering, Heilongjiang Institute of Technology.Harbin, 150050, P.R. China.*
wangxiaoxu0104@163.com

Abstract

This thesis develops efficiency optimization control strategies for three phase induction motors with Hall sensor. This thesis compares the different control strategies include open-loop voltage-mode control of hard-commutation scheme, open-loop voltage-mode control of soft-commutation scheme, and closed-loop current-mode control scheme, and analyzes the current response and overall efficiency. This thesis also develops a low-cost and high efficiency sensorless control for three phase induction motors drives. The proposed scheme detects the back-EMF zero-crossing-point (ZCP) to realize current commutation without Hall sensor. An adjustable blanking time control method is used to ensure correct detection of the ZCP. When using sensorless commutation control, the fan motor can start-up smoothly and operate under wide speed range, moreover, the overall efficiency is almost the same to the results of control scheme with Hall sensor.

Keywords: *Open-loop voltage-mode control, Induction motors, Hall sensor*

1. Introduction

With fast advance in technology, it is essential for the electronic products to be elaborated and sophisticated, and the internal functions are various and high speed. A common problem associated with modern electronic product is forced air cooling. The easiest way with low cost for forced air cooling is induction motors installations. The phase windings of induction motors can be categorized as three-phase, their flux distribution can be either sinusoidal or trapezoidal[1-2].

A common problem associated with the sensorless motor drive system is its starting performance. Using above sensorless algorithms, the measured signal is too small to make precise position estimation when motor is at standstill or low speed. The most common solution to the problem is the open-loop start-up method from a pre-determined rotor position [3].

The permanent magnet rotor will align to the direction corresponding to the induced magnetic field. With a known initial rotor position, an open loop control with ramp up frequency of injecting current is applied to speed up the motor from standstill. However, especially for the three phase induction motors, it has three phase winding, so the induced stator field is just two opposite directions.

With the rapidly development of integrated circuit, digital motor control systems have been widely implemented with software based on microcontrollers or digital signal processor(DSP). These approaches provide flexibility and are suitable for motor drive applications.

The proposed control schemes have been implemented on a single-chip DSP controller(TMS320LF2407A) to verify the performance and feasibility for three phase

ISSN: 2005-4297 IJCA

induction motors. Experimental verification has been carried out on a three phase induction motors control system[4-6].

2. Motor Athematical Modeling

The induction motors, along with an appropriate power converter and either speed or position feedback, have become popular in many sophisticated control applications. The proper design and compensation of such system requires an accurate mathematical model with all of the components of the system. This research proposes a simple modeling method to meet the characteristics of three phase induction motors, and to investigate both static and dynamic relationship between the driving circuit and the real motor .

Figure 1 shows the schematic of the full-bridge inverter and equivalent modeling for a three phase induction motors. The stator winding can be modeled as a winding resistance in series with a winding inductance and a back-EMF voltage. The voltage equation describing the dynamic behavior of three phase induction motors is given as follow[7-8]

$$v = L_s \frac{di}{dt} + iR_s + v_{emf} \tag{1}$$

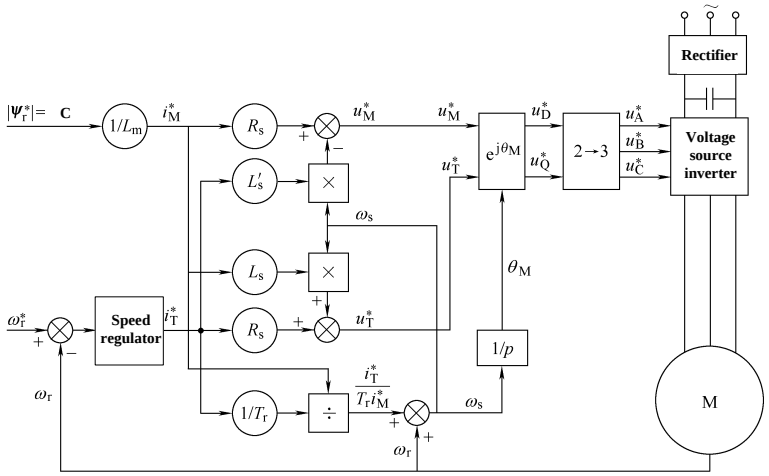

Figure 1. Schematic of the Full-bridge Inverter and Equivalent Modeling for a Three Phase Induction Motors

where v and i are the phase voltage and phase current, respectively. RS and LS are the winding resistance and the winding inductance, respectively. vemf is the back-EMF voltage induced by rotor flux variation and the value is proportional to motor speed and can be computed by

$$v_{emf} = K_E \cdot \omega_r \tag{2}$$

where ωr is the rotor velocity and KE is the back-EMF constant which is associated with the form of nonlinear flux distribution in this application.

For the mechanical system, the developed torque must overcome the inertial acceleration torque, friction torque and the load torque. Therefore, the torque-speed characteristics can be formulated as

$$T_e = J_m \frac{d\omega_r}{dt} + B_m \omega_r + T_L \tag{3}$$

where the inertial acceleration torque is represented by the product of the moment of inertia Jm and the angular acceleration dωr /dt. The load torque referred to the motor shaft, while the friction torque is the product of the rotor velocity and viscous friction coefficient Bm.

Figure 2 is the steady-state current response when using open-loop voltage-mode of hard-commutation scheme. There is a significant current spike at commutation boundary. The dynamic behavior of current response is given as follow

$$i(t) = \frac{v - v_{emf}}{R_s}(1 - e^{-\frac{R_s}{L_s}t}) \tag{4}$$

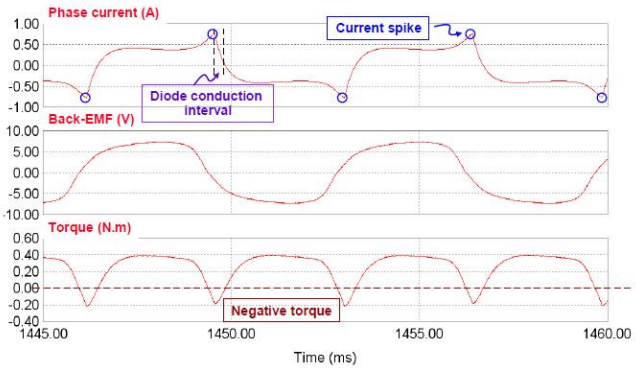

Figure 2. Simulation Result of Step Response at Operation Point of 250 mA

where v is the input voltage of phase winding. R_s and L_s are the series resistance and the series inductance of stator winding, respectively. v_{emf} is the back-EMF induced by rotor flux variation. Owing to the back-EMF seriously drops at commutation boundary, and it results in a great rising slope of current response, that is the current spike. Moreover, due to the winding inductance, the polarity of the phase current cannot be changed instantaneously, so the current will pass through the anti-parallel diode and decrease to zero at commutation boundary. It results in the driving current out of phase with back-EMF and a negative torque is generated, and consequently the overall efficiency is seriously degraded in wide speed control applications for three phase induction motors[9-12].

3. Efficiency Optimization of Three Phase Induction Motors

Due to the machine design and structure, the induced back-EMF in the three phase induction motors is highly nonlinear and contains harmonics. The product of back-EMF and phase current produces the electrical output power. Therefore, it has to consider all the harmonics when calculating output power. The average output power is presented as

$$P_{av} = \frac{1}{T}\int_0^T e(t) \cdot i(t) dt \tag{5}$$

and each back-EMF and phase current is described as

$$\begin{aligned} e(t) &= E_1 \sin \omega t + E_3 \sin 3\omega t + E_5 \sin 5\omega t + \cdots \\ i(t) &= I_1 \sin(\omega t - \phi_1) + I_3 \sin 3(\omega t - \phi_3) + I_5 \sin 5(\omega t - \phi_5) + \cdots \end{aligned} \tag{6}$$

where E_n and I_n represent the peak magnitude of each harmonic of back-EMF and phase current. ϕ_n is the phase difference between each back-EMF and phase current. For maximum output power, each back-EMF and current harmonics should be in phase.

Otherwise, the output power has a negative value during every cycle and average power can not be the maximum possible.

Under this condition, there are many current waveforms may produce the maximum output power. However, there is an optimal current waveform to achieve the maximum

efficiency for three phase induction motors drives. If each harmonic of phase current is same to the back-EMF, the RMS value of phase current is minimum and the corresponding power loss in passive element is minimum. Therefore, in order to realize the maximum efficiency, the phase current waveform should be identical and in phase with the back-EMF.

This research uses the digital PI controller to realize the current-regulation which ensures that the measured stator current tracks the required values accurately and to shorten the transient interval as much as possible. For simplicity, this research uses the digital redesign approach, which determines an equivalent continuous time model of overall system, to use it in the design of a continuous time controller stabilizing the feedback loop and, finally, to turn the continuous time controller into an equivalent discrete time one. The digital redesign has advantage for using some of the well known controller design methods developed for continuous-time analog implementation.

Figure 3 shows the frequency response of system loop gain with analog PI controller and digital PI controller. The system bandwidth is 1.9 kHz and phase margin is 50 degree. Also, the result of analog PI controller is close to the result of digital PI controller, it means that the digital redesign approach is valid and practical. Figure 3.30 shows the step response at operation point 250 mA and the fan motor keeps in standstill. The results are stable and close to 1storder response, and the rise time of current response is 190μs. This implies that the system bandwidth is approximate 1.84 kHz by approximation method of 1st-order response.

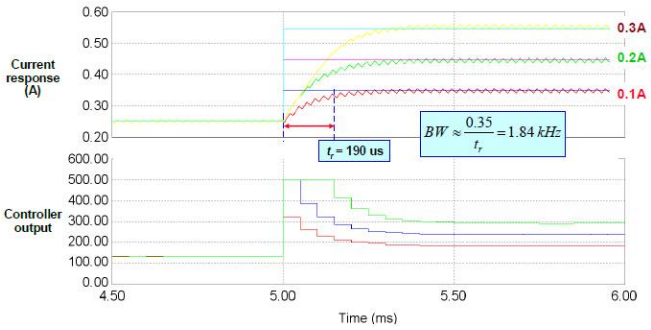

Figure 3. Simulation Result of Step Response at Operation Point of 250 mA

4. Open-Loop Voltage-Mode Control With Hall Sensor

According to the above description, the block diagram of open-loop voltage-mode sensorless control for three phase induction motors is shown in Figure 4. The phase voltage is sampled for detecting the ZCP of back-EMF to produces a sequence of commutation signal.

There is a mode selector to switch the start-up mode and sensorless mode. These commutation signals are used to estimate the motor speed and to determine the conducting time and the direction of driving current. Figure 5 shows the fan motor smoothly starts without Hall sensor, and the start-up time is approximately 0.3 seconds. Then, the fan motor is switched to the sensorless mode, and eventually accelerates to 4000 RPM. Figure 6 shows the steady state waveform of sensorless control at 4000 RPM. When the current decreases to zero, the nonexcited voltage is equivalent to back-EMF voltage, and ZCP detection produces the commutation signal for controlling the next commutation cycle. Similarly, Figure 7 shows the simulation result of start-up procedure from standstill to 1000 RPM, and Figure 8 shows the steady state waveform when the fan motor is operated at 1000 RPM.

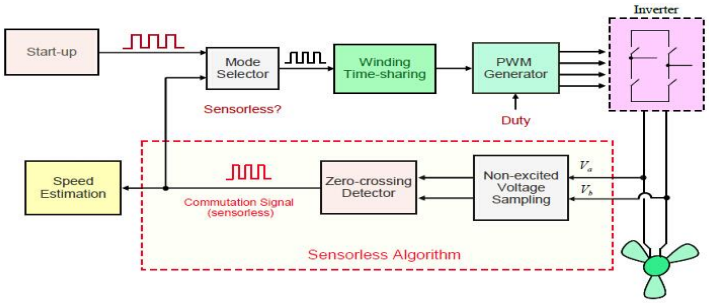

Figure 4. Block Diagram of Open-loop Voltage-mode Sensorless Control for Three Phase Induction Motors

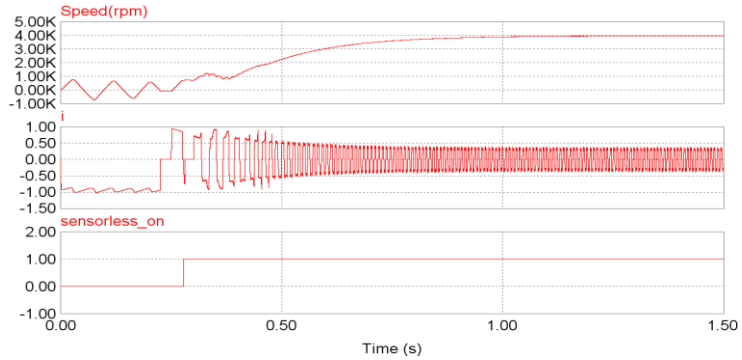

Figure 5. Sensorless Start-up Control from Standstill to 4000 RPM

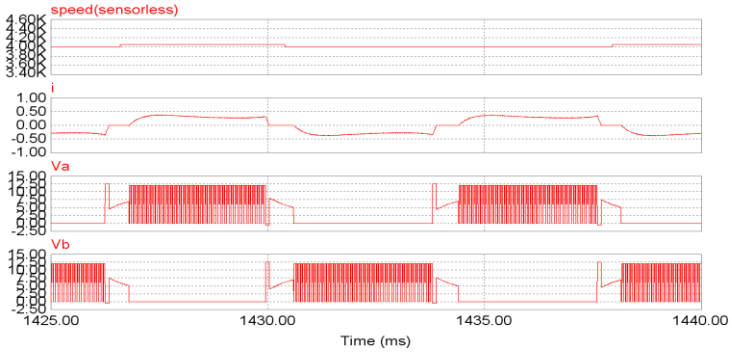

(a)

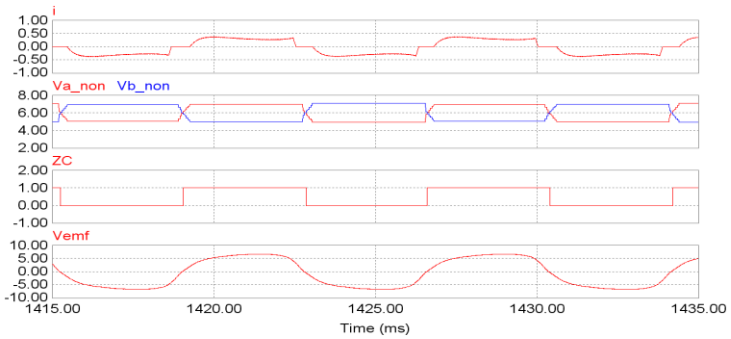

(b)

Figure 6. Simulation Results of Sensorless Control at 4000 RPM (a) Steady StateWaveforms of Phase Current and Phase Voltage and (b) Non-excited Voltage Sampling and ZCP Detection

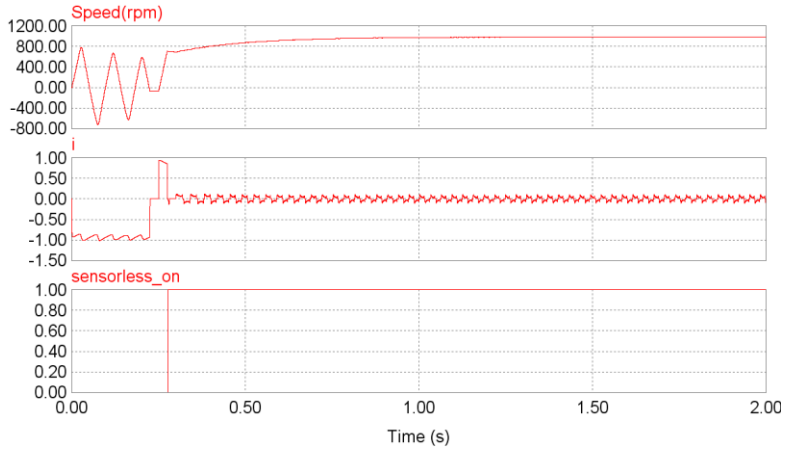

Figure 7. Sensorless Start-up Control from Standstill to 1000 RPM

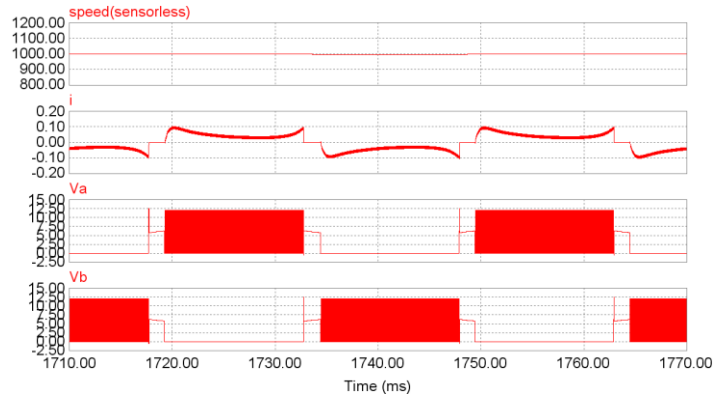

Figure 8. Simulation Results of Sensorless Control at 1000 RPM (a) Steady State Waveforms of Phase Current and Phase Voltage

5. Experimental Result Analysis

The current-loop sensorless control scheme can be verified by computer simulation with proposed model. Figure 9 shows the simulation results of current-loop control at different speed operation. It can be seen that the current spike at commutation boundary has been removed, and the current response closely follows current command. Besides, by look-up table of back-EMF, the current waveform retains the characteristic of corresponding back-EMF. Figure 10 shows the statistics curves for RMS value and peak value of phase current with different control schemes. For entire speed control range, both of RMS value and peak value is lower when using closed-loop current-mode control. That is to say, the closed-loop current-mode control of sensorless motor drive is a low cost and high efficiency solution for three phase induction motors.

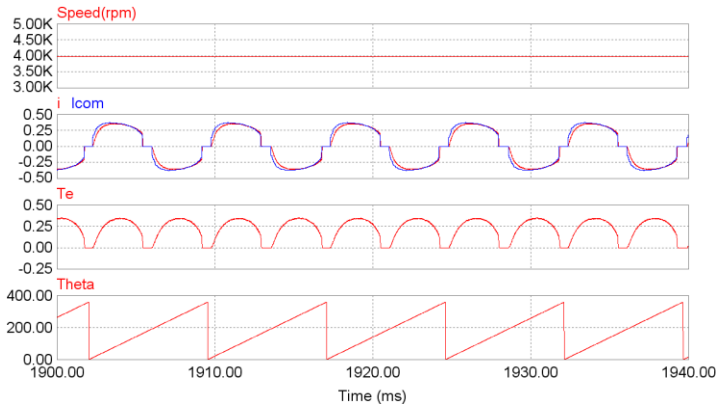

(a)

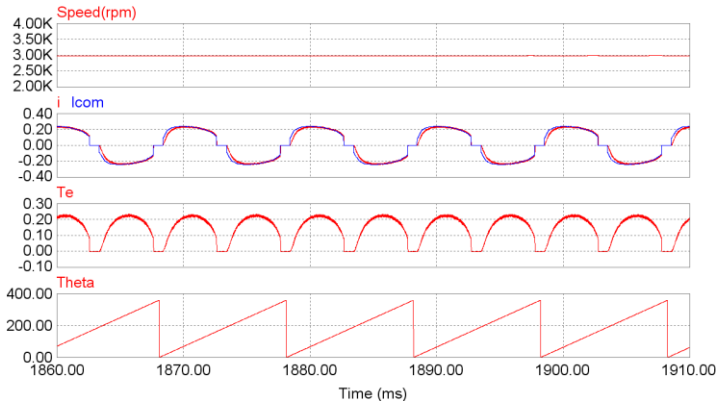

(b)

Figure 9. Simulation Results of Current-loop Control at Different Speed Operation (a) 4000RPM, (b) 3000 RPM

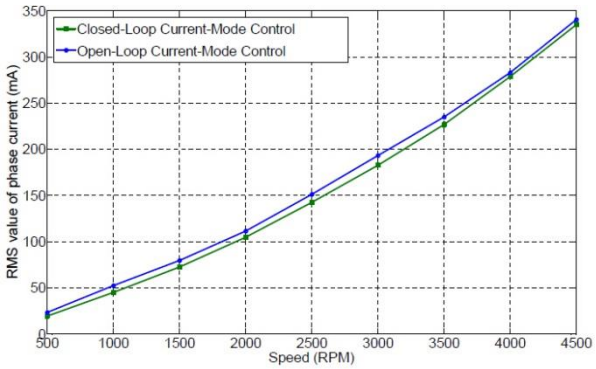

Figure 10. Statistics Curves for Different Control Schemes RMS Value of Phase Current

6. Conclusions

This work presents the efficiency optimization control for three phase induction motors with Hall sensor. The control scheme has been verified by computer simulation based on the proposed model. Besides, the drive system is implemented by DSP, and some experimental results have been shown to verify the performance and feasibility.

This thesis presents an efficiency optimization control scheme for three phase induction motors with linear Hall sensor. To produce the maximum output power, the each back-EMF control system with Hall sensor on a digital signal processing hardware platform.

The DSP controller performs the real-time control algorithms, start-up control and current-loop control, etc. Then, the practical realization issues and analyses of experimental results are also presented.

In summary, this work presents efficiency optimization control for three phase induction motors with Hall sensor. The developed control strategies are first verified by proposed model, and then fulfill on a real three phase induction motors with Hall sensor based on DSP controller.

References

[1] L. Sun, Q. Fang and J. Shang, "Drive of three phase Brushless DC Motors Based on Torque", IEEE Trans. Magnetics, vol. 43, no. 1, **(2007)**, pp.46–50.
[2] R. D. Rubaai and M. D. Kankam, "Development and Implementation of an Adaptive Fuzzy-Neural-Network Controller for Brushless Drives", IEEE Transactions on Industry Applications, vol. 38, no. 2, **(2002)**, pp.441–447.
[3] Y. C. Son, K. Y. Jang and B. S. Suh, "Integrated MOSFET inverter module of low-power drive system", IEEE Trans. Ind., vol. 44, no. 3, **(2008)**, pp.878–886.
[4] C. Xia, Z. Li and T. Shi, "A control strategy for four-switch three phase brushless dc motor using single current sensor", IEEE Trans. Ind. Electron, vol. 56, no. 6, **(2009)**, pp.2058–2066.
[5] G. J. Su and J. W. Mckeever, "Low-cost sensorless control of brushless DC motors with improved speed range", IEEE Trans. Power Electron, vol. 19, no. 2, **(2004)**, pp.296–302.
[6] C. T. Pan and E. Fang, "A phase-locked-loop-assisted internal model adjustable-speed controller for BLDC motors", IEEE Trans. Ind. Electron, vol. 55, no. 9, **(2008)**, pp.3415–3425.
[7] A. Sathyan, N. Milivojevic, Y. J. Lee, M. Krishnamurthy and A. Emadi, "An FPGA-based novel digital PWM control scheme for BLDC motor", IEEE Trans. Ind. Electron, vol. 56, no. 8, **(2009)**, pp. 3040–3049.
[8] Y. Liu, Z. Q. Zhu and D. Howe, "Commutation torque ripple minimization in direct-torque-controlled PM brushless dc drives", IEEE Trans. Ind. Electron, **(2007)**, vol. 43, no. 4, pp.1012–1021.
[9] H. F. Lu, L. Zhang and W. L. Qu, "A new torque control method for torque ripple minimization of BLDC motor with un-ideal back EMF. IEEE Trans", Power Electron , vol. 23, no. 2, **(2008)**, pp.950–958.
[10] K. Wei, J. J. Ren, F. H. Teng and Z. C. Zhang, "A novel PWM scheme to eliminate the diode freewheeling in the inactive phase in BLDC motor", Proc. IEEE Power Electron. Conf., **(2004)**, pp.2282–2286.
[11] W. Chen, C. L. Xia and M. Xue, "A torque ripple suppression circuit for brushless DC motors based on power dc/dc converters", Proc. IEEE, Ind. Electron. Appl, Conf., **(2008)**, no. 3, vol. 34, pp.1453–1457.
[12] F. Rodriguez and A. Emadi, "A novel digital control technique for brush adjustable-speed controller for BLDC motors", IEEE Trans. Ind. Electron, vol. 56, no. 6, **(2009)**, pp. 2058–2062.

